43rd Aerospace Sciences Meeting and Exhibit
January 10-14, 2005 / Reno, NV

Hybrid Simulations of Richtmyer-Meshkov Instability

Bruce Fryxell* and Suresh Menon†
Georgia Institute of Technology, Atlanta, GA, 30332-0150, USA

We present a new hybrid method for direct numerical simulations (DNS) and large-eddy simulations (LES) of complex flows containing moving strong discontinuities and shocks. This hybrid method combines a high-order smooth flow solver with a high-resolution shock capturing method to optimize the best features of the two methods. The solution is free from numerical oscillations near strong discontinuities, and at the same time, resolves fine-scale turbulent features in the smooth flow region with minimal dissipation. This hybrid scheme automatically switches between the shock capturing and the smooth flow algorithm by computing a smoothness parameter. The combined methodology is used to simulate the classical Richtmyer-Meshkov (RM) instability in both 2D and 3D to demonstrate the new capability.

I. Introduction

Both direct numerical simulations (DNS) and large-eddy simulations (LES) have become well-established tools to simulate turbulent flows. However, nearly all reported studies have focussed on DNS and LES of flows that did not include discontinuities, such as shock waves. A major problem for DNS and/or LES of flows with shocks (especially, moving shocks) is that algorithms developed for smooth flows (i.e., flows without discontinuities) are numerically unstable in regions containing strong shocks. Shock capturing schemes developed for steady-state applications have not shown potential for resolving unsteady shear flows in conjunction with shock waves, e.g., shock-shear interactions. On the other hand, time and space accurate schemes developed for DNS and LES[1,2,3,4] cannot be easily extended to deal with flows containing strong discontinuities.

Recent efforts[5] have demonstrated a mixed scheme that combines a central difference algorithm with a WENO upwind scheme for DNS application. Primarily, 2D simulations were conducted using this technique. In the present study, we will demonstrate a new hybrid approach in both 2D and 3D that combines a high-resolution shock capturing algorithm with a high-order smooth flow algorithm. The combined scheme was developed to be applicable for both DNS and LES applications. To demonstrate this approach we focus on simulation of a Richtmyer-Meshkov instability, since it contains all the fundamental features of interest. Richtmyer-Meshkov instability[6,7,8] develops when an interface between two materials with different densities is accelerated impulsively, for example, by the impact of a shock wave and results in the mixing of the two materials. This instability plays a fundamental role in supersonic flows under a wide variety of length and time scales, ranging from tiny inertial confinement fusion capsules to astronomical events, such as supernova explosions. We also present the results for a simpler test problem, the propagation of a one-dimensional shock wave through a sinusoidally-varying density profile, which is particularly relevant to the problem of shock induced turbulence.

*Senior Research Scientist, School of Aerospace Engineering, AIAA Member.
†Professor, School of Aerospace Engineering, AIAA Associate Fellow.

In the following section, we describe the numerical techniques used for this study. These include the baseline hydrodynamic method used for the smooth portions of the flow, the shock capturing method, and the technique we use to combine the two methods into a hybrid code. The third section will describe the calculations used to test the hybrid method and show preliminary results. The final section contains some concluding remarks and describes future directions for this research.

II. Numerical Methods

In this section we describe a new hybrid code, which couples a high-order finite-volume method with a high-resolution shock capturing algorithm. The shock capturing technique is used only near shocks and contact discontinuities, while the high-order method handles the smooth regions of the flow. The code used for this study is a well-established DNS/LES solver (LESLIE3D) developed for scalar mixing and combustion application in gas turbine and scramjet engines.[2,9] The baseline solver is a predictor-corrector finite-volume scheme that is nominally second-order accurate in both space and time. A fourth-order accurate spatial scheme is also present in this code, and is typically employed in both DNS and LES to obtain final statistics. Although the code has full Navier-Stokes and LES capability, we limit the discussion here to inviscid DNS test problems that illustrate the properties of the new hybrid technique. To describe the hybrid scheme we consider the Euler equations in a one-dimensional Cartesian geometry as

$$\frac{\partial U}{\partial t} + \frac{\partial F}{\partial x} = 0, \tag{1}$$

where U is the vector of conserved quantities (density, momentum, and energy) and F is the flux vector.

A. Smooth-Flow Solver

The smooth-flow finite-volume (SM-FV) solver in the code can be expressed as

$$U_i' = U_i^n - \frac{\Delta t}{\Delta x}\left(F^+_{i+\frac{1}{2}} - F^+_{i-\frac{1}{2}}\right) \tag{2}$$

$$U_i^{n+1} = \frac{1}{2}\left(U_i^n + U_i' - \frac{\Delta t}{\Delta x}\left(F^-_{i+\frac{1}{2}} - F^-_{i-\frac{1}{2}}\right)\right). \tag{3}$$

A method which is second order in both space and time can be obtained by evaluating the fluxes as

$$\begin{aligned} F^+_{i+\frac{1}{2}} &= F^n_{i+1} \\ F^-_{i+\frac{1}{2}} &= F'_i \end{aligned} \tag{4}$$

The quantity F_i is evaluated using the cell-centered values of U in zone i. Alternating between forward and backward spatial differences of the flux derivatives between the predictor and corrector steps results in a central difference scheme.

An extension to the above method which is accurate to fourth order in space and second order in time is also present in this code.[10] The only difference is that the fluxes are now computed according to the formulas

$$\begin{aligned} F^+_{i+\frac{1}{2}} &= \frac{1}{6}\left(2F^n_i + 5F^n_{i+1} - F^n_{i+2}\right) \\ F^-_{i+\frac{1}{2}} &= \frac{1}{6}\left(2F'_{i+1} + 5F'_i - F'_{i-1}\right). \end{aligned} \tag{5}$$

Either the second-order or fourth-order SM-FV method in LESLIE3D can be used with the hybrid method. Because of its smaller numerical dissipation, the fourth-order method is more accurate, but less robust. However, as part of the hybrid method, this is not a significant drawback, since the shock capturing scheme will take over in any regions of the flow where numerical instability would otherwise be a concern.

B. Shock Capturing Method

The scheme we use for shock capturing is the Piecewise-Parabolic Method (PPM) of Colella and Woodward.[11] This method has been widely used, particularly for astrophysics calculations, where strong shocks appear on a regular basis. The implementation used here is based on the PROMETHEUS code,[12] which is also the basis of the hydrodynamic solver in the FLASH code,[13] developed at the University of Chicago as part of the DOE ASCI Alliance Program. The code has been used by many groups throughout the world and has been extensively verified and validated.[14,15]

PPM is a high-order extension of Godunov's method.[16] The algorithm was designed specifically to produce accurate solutions of flows with sharp discontinuities through the use of nonlinearity and "smart" dissipation algorithms. It also performs very well in smooth flows. Godunov's approach is to calculate the fluxes in the gas dynamic equations by solving Riemann's problem at each zone interface. This produces an upwind-centered flux and also introduces nonlinearity into the difference equations. This nonlinearity permits the method to calculate narrow discontinuities without generating spurious oscillations. Godunov's method assumes a piecewise-constant profile of each variable. In other words, each variable in each zone is constant in space. This limits the accuracy of the scheme to first order.'

A formalism for extending Godunov's method to higher order was developed with the MUSCL scheme,[17] in which second-order accuracy in both space and time is achieved by representing the flow variables as piecewise-linear instead of piecewise-constant functions. This is analogous to switching from the rectangle rule to the trapezoidal rule for numerical integration of a function. Another major advance of MUSCL was the incorporation of monotonicity constraints instead of artificial viscosity to eliminate oscillations in the flow.

PPM takes the next logical step by representing the flow variables as piecewise-parabolic functions. This corresponds to switching to Simpson's rule for numerical integration. Although this could lead to a method which is accurate to third order, PPM is formally accurate to only second order in both space and time. A fully third-order method provides only a slight additional improvement in accuracy but results in a significant increase in the computational cost of the method. However, the most critical steps are performed to third-order or fourth-order accuracy, resulting in a method which is considerably more accurate and efficient than most second-order codes using typical grid sizes.

We include here only a brief description of the algorithm. A detailed discussion of the PPM algorithm is beyond the scope of this paper. A thorough description of the method is contained in the above references.

Like the smooth-flow solver, PPM is a finite-volume method, and therefore, it uses cell-average values of the conserved quantities as input data. The first step in the solution is to construct left and right interface values of the primitive variables (density, velocity, pressure, and mass fraction) for each computational zone from the zone-average values. For PPM we use a cubic polynomial to obtain fourth-order accuracy. This interpolation is subject to monotonicity constraints to prevent spurious oscillations from developing in the solution. After completion of the interpolation, each primitive variable in each zone has associated with it a zone average value and left and right interface values. It is now possible to construct a parabola which passes through the two interface values and which also has the correct average value for the zone.

These interface values and parabolae are only preliminary. There are situations in which they must be modified in order to obtain acceptable results. The first modification to be applied is to check for the presence of shock fronts which are too narrow. Due to the small amount of numerical dissipation in PPM and the self-steepening property of shock waves, the algorithm can produce shocks which are too narrow to be treated accurately. The result is unphysical post-shock oscillations which can corrupt the entire solution.

To prevent this from happening, additional dissipation must be added to the scheme. However, instead

of resorting to the traditional technique of adding an artificial viscosity to the difference equations to smear out the shock, another procedure, called flattening, is employed. It is much easier to keep the effects of this dissipation localized to regions near shocks than with artificial viscosity. The method actually measures the number of zones contained within each shock, and turns on only for shocks which are too narrow. In this way, it is able to maintain a shock width of one to two zones.

This procedure modifies the interface values for a zone by taking a linear combination of the interface values computed above with those which would have been obtained using a first-order Godunov scheme. For the first-order method, which uses a piecewise-constant distribution, the interface values are just equal to the zone average value. The scheme becomes first-order accurate in regions near shocks. However, since the concept of order applies only to smooth flow, this is not a concern. All shock capturing schemes are first-order accurate in the vicinity of discontinuities.

The other situation in which the interface values must be modified is if any point on the parabola falls outside the range determined by the two interface values. This can occur either near a steep gradient or near a local maximum or minimum. In the later case, both interface values are set to the cell-average value. In the former case, the slope of the parabola at one interface is set to zero, and the opposite interface value is adjusted to maintain the same cell-average value.

The next step is to compute the fluxes of the conserved quantities through the left and right interface of each zone. The zone interface values computed by the above procedures can not be used directly to compute the fluxes. First of all, there may be two values of each variable associated with each interface. Second, since these values are centered at the old time step, using them would provide forward differencing in time, which is numerically unstable. Instead, the fluxes are computed by solving Riemann's problem at each zone interface.

Riemann's problem determines the evolution of two constant states that are initially separated by a discontinuity. This is slightly different from the situation here in which the discontinuity at the zone interface separates two states with parabolic distributions. Because of this, it is necessary to construct effective left and right states which will produce a suitable solution to the Riemann problem. Consider the zone interface at $\xi_{i+\frac{1}{2}}$. The simplest choice for the left and right states would be the zone average values in zones i and $i+1$. However, this would give results identical to Godunov's method, and all of the work described above would have been wasted.

To produce higher-order accuracy, a more complicated approach is needed. Since all signals travel with a finite speed in gas dynamics, not all of the material within zones i and $i+1$ can influence the zone interface during the time step (assuming that the CFL number is less than one, as required for numerical stability). The first step is to determine the domain of dependence of the zone interface during the time step. This is accomplished by tracing characteristics backward in time from the zone interface at time $n+1$ to the ξ axis at time n. Only the material between the point of intersection of the characteristic with the ξ axis and the zone interface can influence the interface during the time step. The amount of material within this region is easily computed by integrating the parabolic distribution.

The next step is to solve Riemann's problem at each zone interface using these effective left and right states. Riemann's problem has the effect of converting the left and right states, which in the above procedure represent spatial averages, into values which represent averages in time over the interval t to $t+\Delta t$. The values obtained are used to calculate the flux of the conserved quantities through the zone interfaces. The final step is to use these fluxes to update the conserved quantities in conservative finite difference equations, which can be written as

$$U_i^{n+1} = U_i^n - \frac{\Delta t}{\Delta x}\left(F_{i+\frac{1}{2}} - F_{i-\frac{1}{2}}\right) \tag{6}$$

C. Hybrid Method

There are a number of advantages to using a hybrid method rather than either of the methods described above by itself. First, the base-line SM-FV method works very well in smooth flows that contain complex

shear flows. However, it cannot handle discontinuities, or at least produces significant unphysical oscillations in the vicinity of these discontinuities. One the other hand, PPM can handle both discontinuities and the smooth portions of the flow reasonably well. However, the fourth-order spatial accuracy of the SM-FV solver should provide more accurate resolution of shear flow in smooth regions. There is also some concern that the upwind dissipation in PPM may lead to an un-physical rate of decay of turbulent flow fields. This is a somewhat controversial issue and one which we will be able to address with the hybrid method.

In addition, the computational cost to update each grid point is much larger for PPM than for the fourth-order SM-FV solver (by a factor of four). Much of the cost of PPM goes into the mechanisms for handling discontinuities, and all of this work is wasted in the smooth portions of the flow. Thus, a substantial computer time saving can be achieved by using PPM only in a small portion of the grid. Finally, the LES algorithms in LESLIE3D have been thoroughly tested and validated, and their behavior is well understood. Therefore, extension of the hybrid scheme to LES of flows with strong discontinuities should be relatively straight-forward.

In order to construct the hybrid method, it is necessary to construct a measure of the smoothness of the solution. For this purpose, we use an estimator similar to one proposed by Löhner[18] as a refinement criterion in adaptive mesh methods. We begin by defining a switch S by

$$S_i = \frac{|Q_{i+1} - 2Q_i + Q_{i-1}|}{|Q_{i+1} - Q_i| + |Q_i - Q_{i-1}|}, \tag{7}$$

where Q can be any variable of interest. For the present study, we use both density and pressure, and take the maximum of the two values. To prevent switching on numerical noise, we set $S_i = 0$ if either the numerator or the denominator divided by Q_i is less than 0.01. For multidimensional flows, the maximum value of S_i for each coordinate direction is used. Although one could also construct a switch taking into account all cross derivatives of Q, this possibility has not yet been investigated.

In any cell in which the value of S_i exceeds some threshold, typically 0.5, PPM is used to construct the fluxes through each face of that cell. For each cell bordering a cell in which PPM is needed, the average of the PPM flux and the SM-FV flux is used. In the remainder of the grid, the SM-FV flux alone is used. Since this procedure produces only one flux value at each zone interface, the conservative nature of the method is maintained.

The conserved quantities are updated by inserting the appropriate fluxes into equations (2) and (3). For interfaces which use the PPM flux, the same flux is used for both the predictor and corrector steps. The result of this procedure is identical to that obtained if PPM were used by itself.

In the following discussion, we will refer to the combination of PPM with the second-order SM-FV method as the second-order hybrid (O2H) scheme and the coupling of PPM to the fourth-order method as the fourth-order hybrid (O4H) scheme, even though this does not represent the overall order of accuracy of the hybrid method.

III. Results

A. Shu-Osher Test Problem

The Shu-Osher problem involves a one-dimensional shock front propagating into a sinusoidal density distribution. Its purpose is to test the ability of a code to accurately compute shocks and short-wavelength smooth variations in the same calculation, and thus it is an ideal test problem for the hybrid method. It is particularly relevant to the problem of shock-induced turbulence.

The initial conditions for this problem are as follows. The density profile is given by

$$\rho(x) = \begin{cases} 3.857142 & x < 2 \\ 1 - 0.2\sin(5x) & x \geq 2 \end{cases}. \tag{8}$$

The pre-shock pressure and velocity are 1 and 0, respectively. The post-shock values for pressure and velocity are 10.333333 and 2.629369, and the adiabatic index of the gas is 1.4. The results are plotted at a time of 1.872. Although there is no analytic solution for this problem, it is possible to obtain a converged solution to which the results can be compared. Our reference solution was obtained using PPM with a grid resolution of 1600 points. The solution consists of a shock, followed immediately by a region of rapid oscillations. Fairly high grid resolution is required to compute this region accurately. Behind this is a region of longer-wavelength oscillations traveling to the left, which steepen into shocks, forming a characteristic N-wave pattern.

Both the second-order and fourth-order SM-FV methods in the original LESLIE3D code by themselves have significant difficulty with this problem because of the presence of the shocks and the very steep profiles in the high-frequency oscillations. The difficulty with the rapid oscillations could be solved by using finer grids, but this will not help with the shocks.

The results for both the O2H and O4H methods at a grid resolution of 400 points are shown in figure 1. The red squares show the places where the PPM fluxes were used. At the blue circles, the SM-FV fluxes were used. The average of the two fluxes was used at the points represented by the green triangles. Also shown is the reference solution, represented by the solid black line. For both cases, the structure of the first three N-waves is well represented, but the amplitude of the high-frequency oscillations behind the shock is significantly reduced. The O4H method does slightly better than the second-order method, as expected. For the O2H case, there is also a significant error in the structure of the flow between the N-waves and the high-frequency oscillations. The PPM fluxes are needed at all the shock locations, as well as at the maxima and minima of the high-frequency oscillations. At the final time, for the O2H case, the PPM fluxes are used at 47 grid points, and the average of the two fluxes are used at 31 grid points. For the O4H method, PPM is needed at 65 grid points and the average of the fluxes at 27 points. The fraction of points needing PPM fluxes increases with time as the flow becomes more complex.

The results obtained on an 800 point grid are shown in figure 2. The O2H method still shows a significant loss in amplitude of the high-frequency oscillations, although it is getting close to the reference solution. There are also some unphysical oscillations just to the left of the high-frequency region. At this resolution, the O4H method is very close to the reference solution. The fraction of grid points requiring the PPM fluxes is now considerably less. There are enough grid points that the high-frequency oscillations are beginning to look like smooth flow, and most of this region can be treated accurately with the SM-FV scheme. The O2H method requires PPM at only 16 grid points and averaged fluxes at 20 grid points and the O4H method uses PPM at 20 points and averaged fluxes at 22 points.

The results obtained with 1600 points are virtually identical (and therefore, not shown) to the reference solution except for some small oscillations just to the left of the high-frequency region in the O2H calculation. The PPM fluxes are now used only at the shocks. The high-frequency oscillations have become smooth enough to be treated entirely by the SM-FV method. The O2H method uses PPM fluxes at only 10 grid points and averaged fluxes at 8, and for the O4H case, PPM fluxes were needed at just 13 grid points, with 10 zones using averaged fluxes.

A closeup view of the high-frequency region on the 800 point grid is shown in figure 3 for both the second-order and fourth-order cases. The solid line represents the PPM solution, also using 800 grid points. At this resolution, the pure PPM solution is clearly better than the O2H solution. However, the O4H solution is better than the pure PPM solution. The amplitude of the peaks is slightly higher (closer to the reference solution), and the oscillations are more nearly sinusoidal. The nonlinear filters in the PPM method, such as the monotonicity, clip the peaks and distort the waveform slightly. These effects are absent in the fourth-order hybrid results.

B. Richtmyer-Meshkov Instability

The Richtmyer-Meshkov (RM) instability is a close relative of the Rayleigh-Taylor instability, which occurs when an interface between two materials of different density is continuously accelerated, such as by the force of gravity. For the RM instability, the interface is accelerated impulsively, usually by the impact of

a shock. In the linear regime, the Rayleigh-Taylor instability grows exponentially. The RM instability, on the other hand, grows linearly. This is a good validation problem for numerical codes, since there has been considerable experimental and analytical work with which to compare. It also demonstrates a code's ability to handle both shocks and turbulence in the same calculation, making it ideal to test the properties of the hybrid method.

The particular setup used here was chosen to match an experiment performed on the Nova Laser at the Lawrence Livermore National Laboratory. It has been studied extensively, both analytically and numerically. For a complete description of the experiment, as well as comparisons with analytical and numerical work, see Holmes *et al.*[19] The initial configuration consists of a tube of dimension 0.04 x 0.01 cm. At the left of the tube is a layer of foam at a density of 0.12 g cm^{-3}. At the right is a layer of Be at a density of 1.7 g cm^{-3}. A sinusoidal perturbation with an amplitude of 0.001 cm was machined into the interface between the two materials. The laser generates a shock with an overpressure of 300, which propagates from the Be into the foam, accelerating the interface to the left. The experiment was designed to be two-dimensional, so a two-dimensional simulation is appropriate here. However, since our eventual goal is to conduct 3D DNS and LES studies, some 3D RM simulations were also conducted and reported below.

1. Two-Dimensional RM Instability

Figure 4(a) shows the temperature profile obtained with PPM on a 240 x 60 two-dimensional grid at time 9.6 x 10^{-9} s. The impact of the shock causes the interface to undergo a 180^o phase inversion. The perturbation, originally pointing to the right, turns into a finger pointing to the left. The instability develops into the characteristic bubble and spike morphology, with a high-density narrow spike topped by a mushroom cap growing to the left in the center of the tube and low density bubbles at the edges expanding to the right. The instability has developed well into the nonlinear phase. The shock becomes very distorted by the interface, but after a short time, becomes nearly planar again. In the figure, it is located between the dark blue and orange regions near the left edge of the grid. A diamond shaped pattern of contact discontinuities forms between the shock and the interface. These discontinuities are subject to Kelvin-Helmholtz instabilities, which can be seen in higher resolution simulations. A complex series of waves develops in the light blue region at the right of the grid. These waves interact with each other and reflect off the top and bottom of the grid, forming interesting patterns.

The results obtained with the O2H method are shown in figures 4(b) and (c). The temperature, plotted in figure 4(b), is virtually identical to that obtained using PPM alone. The growth rate of the instability, the location of the shock and contact discontinuities, and all other major features of the flow are the same. The small differences that can be seen are easily attributable to the growth of small perturbations in a very unstable flow. The regions of the grid where the PPM fluxes and the SM-FV fluxes were used is plotted in figure 4(c). The PPM fluxes are used in the red areas, the SM-FV fluxes are used in the blue areas, and the average of the two was used in the portions colored green. The PPM fluxes are required mainly at the shock front, at the contact discontinuities between the shock and the interface, along the interface, and along the waves which develop upstream of the interface. The rest of the flow can be treated accurately with the SM-FV method. The fraction of the grid requiring PPM or averaged fluxes increases as the calculation proceeds. At this final time, the SM-FV fluxes can be used in all but about 21% of the grid.

Figure 5 shows the results obtained with the O4H method. Again, all of the main features of the flow are reproduced. The locations in the grid where the PPM fluxes are required is pretty much the same as for the O2H method, although the fraction of the grid requiring PPM or averaged fluxes has now increased to 23%.

The results obtained on a 480 x 120 point grid are shown in figure 6 for the PPM and O4H methods. The main features of the flow are very similar to those obtained on the coarser grid. The location of the shock, the growth rate of the instability, and the diamond shaped pattern of contact discontinuities are all essentially unchanged. The primary difference is the development of secondary Kelvin-Helmholtz instabilities along the interface, as well as a general sharpening of all the features in the flow. Both of these are a result of the

increase of the effective Reynolds number of the calculation as the grid size increases. Again, all the main features of the flow are preserved. There is a somewhat larger variation in the shape of the mushroom cap than in the previous set of calculations. As the effective Reynolds number of the calculation increases, one would expect the small perturbations resulting from using different hydrodynamic methods to become more significant. At this higher resolution, the regions of the grid requiring PPM are confined more closely to the interface and to the waves generated by the instability. The fraction of the grid requiring PPM or averaged fluxes has decreased to 17% for O2H and 18% for O4H.

Figures 7(a) and (b) show the results obtained on a grid of 960 x 240 zones for the PPM and O4H methods, respectively. The primary differences in this calculation are an increase in complexity in the structure of the roll up at the edges of the mushroom cap and an additional sharpening of all the features. With decreasing numerical dissipation, any small numerical perturbations to the flow, such as those imposed by moving a curved surface across a rectangular grid, can grow more easily. As a result, the small structures generated differ more between the three methods at high resolution. The fraction of the grid in which the PPM fluxes were used has now dropped to 9% for the O2H method and 10% for O4H.

2. Three-Dimensional RM Instability

Although the Richtmyer-Meshkov experiment described above was designed to be purely two-dimensional, we also performed simulations for the same initial conditions in three dimensions (using a fully three-dimensional initial perturbation). The results obtained for PPM and the O4H method on a 240 x 60 x 60 grid are shown in figures 8 (a) and (b), respectively. The structure of the three-dimensional instability is quite different. The finger is considerably broader, and the mushroom cap and the roll-up are less pronounced. The growth rate of the instability is somewhat faster in 3D. This effect has also been seen in experiments. The wave structure to the right of the finger is also very different in the 3D simulations. For the O2H method (not shown), 28% of the grid points required PPM, while 33% of the points used PPM in the O4H calculation. These numbers are somewhat higher than for the two-dimensional calculations at the same resolution.

A set of higher resolution 3D simulations, using a grid size of 480 x 120 x 120, were also conducted and shown in figures 9(a) and (b), for the PPM and O4H methods, respectively. These figures show the central $x - y$ plane of the simulation. The major features of the flow, including the size and shape of the finger, the shock location, and the diamond pattern of contact discontinuities, are very similar to those obtained at lower resolution. The roll-up at the edge of the mushroom cap is better defined now and there is much more structure along the interface. The fraction of grid points requiring PPM fluxes has dropped to 19% and 20% for the O2H and O4H methods, respectively. This is still slightly more than for the two-dimensional simulations at the same resolution.

Finally, figure 10 shows an isosurface of the temperature field in 3D perspective. These figures show the complex structure which develop in three dimension. The viewpoint is looking toward the bubbles. The under side of the mushroom cap is just barely visible. The shock is represented by the blue plane at the left. Notice the disturbace in the shape of the shock caused by the additional waves formed by the instability.

IV. Conclusions

We have presented a new hybrid method for time and space accurate calculations using DNS and/or LES applications. This new hybrid scheme combines a high-order smooth-flow finite volme solver with a high-resolution shock capturing method based on PPM. The result is a scheme which combines the best features of both methods, including the efficient solution of smooth flows with LES capability and the accurate treatment of discontinuities using the PPM algorithm . The method has been shown to work well for a number of test problems in one, two, and three dimensions. It produces nearly identical results to the original PPM code. No significant numerical oscillations are generated by switching between the two schemes. However, in highly unstable flows such as the Richtmyer-Meshkov instability, small perturbations grow and eventually produce noticeable changes in the flow field, especially at high resolution where the

numerical dissipation is small. Even for these complex flows, only a small portion of the grid requires the use of the PPM fluxes to obtain good solutions. This is especially true for large grids.

Although all the test calculations presented above were run in DNS mode, the hybrid code can use all of the LES features of LESLIE3D. These capabilities will be explored in a future paper. In particular, we plan to use the method for flows involving both shocks and turbulence, including both single-mode and multi-mode Richtmyer-Meshkov instabilities.

Acknowledgements

This work was supported by AFOSR and Eglin AFB. Computations were carried out at the DOD HPC centers at ERDC, MS. J. Hackl and F. Genin of the Computational Combustion Laboratory helped in some of these calculations.

References

[1]Menon, S., "Computational and Modeling Constraints for Large-Eddy Simulations of Turbulent Combustion," *Int. Journal of Engine Research*, Vol. 1, 2000, pp. 209–227.

[2]Kim, W.-W. and Menon, S., "Numerical Modeling of Turbulent Premixed Flames in the Thin-Gas Turbine Combuster," *Comb. Sci. and Tech.*, Vol. 143, 1999, pp. 25–62.

[3]Kim, W.-W. and Menon, S., "Numerical Modeling of Fuel-Air Mixing in a Dry Low-Reaction-Zones Regime," *Comb. Sci. and Tech.*, Vol. 160, 1999, pp. 113–150.

[4]Stone, C. and Menon, S., "Parallel Simulations of Swirling Turbulent Flames," *Journal of Supercomputing*, Vol. 22, 2003, pp. 7–28.

[5]Hill, D. and Pullin, D., "Hybrid Tuned Center-Difference-WENO method for large eddy simulations in the presence of strong shocks," *Journal of Computational Physics*, Vol. 194, 2004, pp. 435–450.

[6]Meshkov, E. E., "Instability of the Interface of Two Gases Accelerated by a Shock Wave," *Fluid Dyn.*, Vol. 43(5), 1969, pp. 101–104.

[7]Meshkov, E. E., "Instability of a Shock Wave Accelerated Interface Between Two Gases," *NASA Tech. Trans.*, Vol. F-13, 1970, pp. 074.

[8]Richtmyer, R. D., "Taylor Instability in Shock Acceleration of Compressible Fluids," *Commun. Pure Appl. Math.*, Vol. 13, 1960, pp. 297–319.

[9]Sankaran, V. and Menon, S., "LES of Spray Combustion in Swirling Flows," *Journal of Turbulence*, Vol. 3, No. 2, 2002.

[10]Nelson, C. C. and Menon, S., "Unsteady Simulations of Compressible Spatial Mixing Layers," *AIAA-98-0786*, 1998.

[11]Colella, P. and Woodward, P., "The Piecwise Parabolic Method (PPM) for Gas Dynamical Simulations," *Journal of Computational Physics*, Vol. 54, 1984, pp. 174–201.

[12]Fryxell, B., Müller, E., and Arnett, D., "Hydrodynamics and Nuclear Burning," *Max-Planck-Institute für Astrophysik Report 449*, 1989.

[13]Fryxell, B., Olson, K., Ricker, P., Timmes, F. X., Zingale, M., Lamb, D. Q., MacNeice, P., Rosner, R., Truran, J. W., and Tufo, H., "FLASH: An Adaptive Mesh Hydrodynamics Code for Modeling Astrophysical Thermonuclear Flashes," *Astrophysical Journal (Supplement)*, Vol. 131, 2000, pp. 273–334.

[14]Woodward, P. and Colella, P., "The Numerical Simulation of Two-Dimensional Fluid Flow with Stong Shocks," *Journal of Computational Physics*, Vol. 54, 1984, pp. 115–173.

[15]Calder, A., Fryxell, B., Plewa, T., Rosner, R., Dursi, L., Weirs, V., Dupont, T., Robey, H., Kane, J., Remington, B., Drake, R., Dimonte, G., Zingale, M., Timmes, F., Olson, K., Ricker, P., MacNeice, P., and Tufo, H., "On Validating an Astrophysical Simulation Code," *Astrophysical Journal (Supplement)*, Vol. 143, 2002, pp. 201–229.

[16]Godunov, S., "A Finite Difference Method for the Computation of Discontinuous Solutions of the Equations of Fluid Dynamics," *Mat. Sb.*, Vol. 47, 1959, pp. 357–393.

[17]van Leer, B., "Towards the Ultimate Conservative Difference Scheme V. A Second Order Sequel to Godunov's Method," *Journal of Computational Physics*, Vol. 32, 1979, pp. 101–136.

[18]Löhner, R., *Comp. Meth. App. Mech. Eng.*, Vol. 61, 1987, pp. 323.

[19]Holmes, R., Dimonte, G., Fryxell, B., Gittings, M., Grove, J., Schneider, M., Sharp, D., Velikovich, A., Weaver, R., and Zhang, Q., "Richtmyer-Meshkov Instability Growth: Experiment, Simulation, and Theory," *Journal of Fluid Mechanics*, Vol. 389, 1999, pp. 55–79.

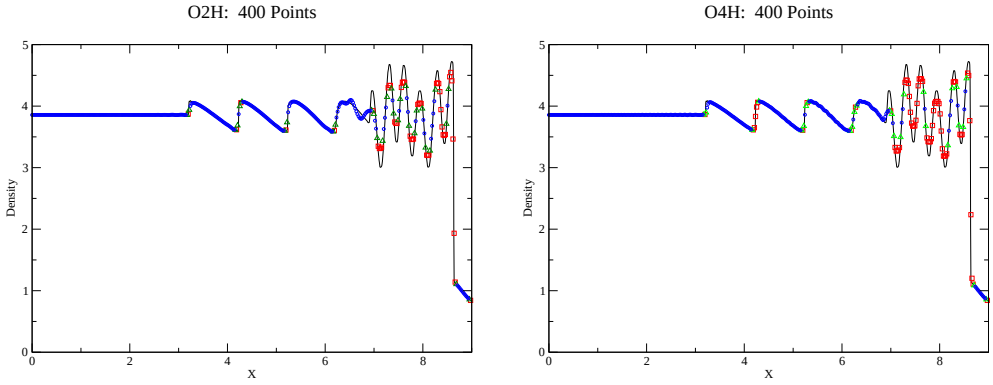

(a) O2H method (b) O4H method

Figure 1. Results for the Shu-Osher problem on 400 points. (i) PPM fluxes: squares, (ii) SM-FV fluxes: circles, and (iii) averaged fluxes: triangles. The solid line is the reference solution obtained using PPM on a 1600 point grid.

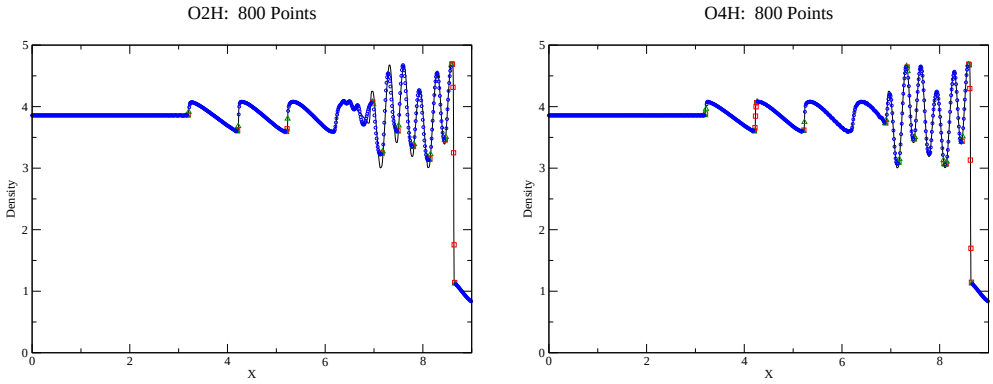

(a) O2H method (b) O4H method

Figure 2. The same as figure 1 at a resolution of 800 grid points.

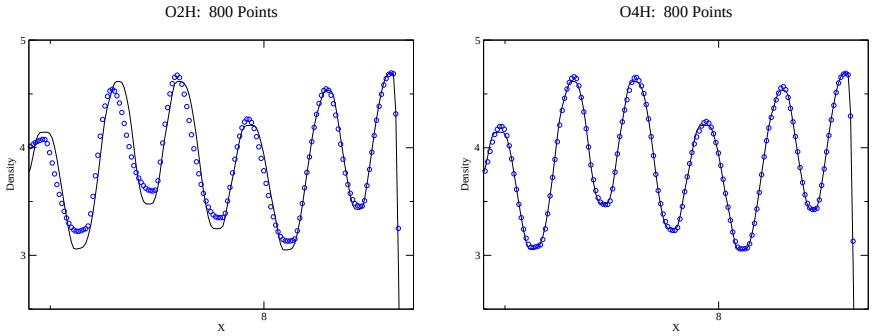

(a) O2H method (b) O4H method

Figure 3. Closeup of the region just behind the shock. The solid line is the pure PPM solution.

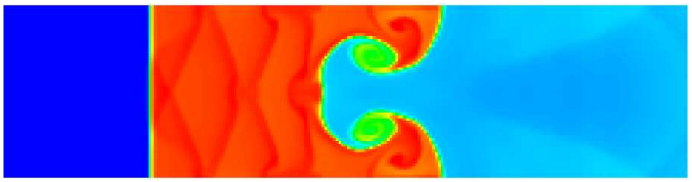

(a) PPM

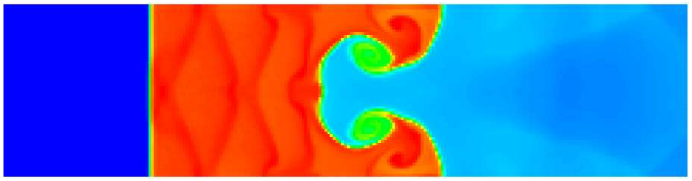

(b) O2H

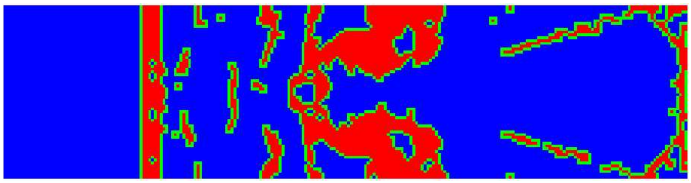

(c) Switch locations

Figure 4. Temperature distribution for a RM simulation obtained using PPM and the O2H method on a grid of 240 x 60 points. The PPM fluxes were used at the points shown as red in (c), the SM-FV fluxes were used in the blue regions, and the regions marked as green show where the average of the two fluxes was used

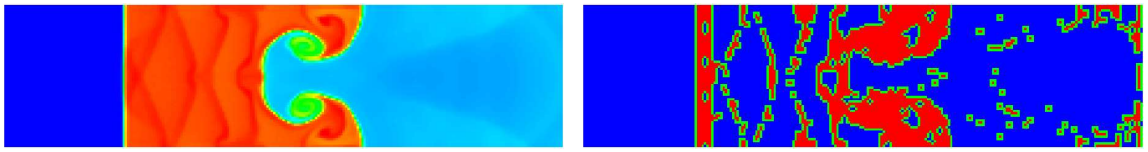

(a) (b)

Figure 5. Same as figure 4 for the O4H method.

(a) PPM (b) O4H method

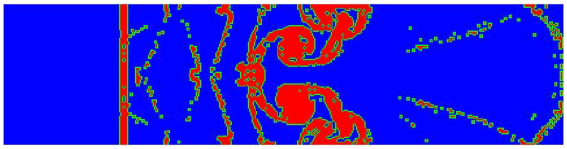

(c) Switch locations

Figure 6. Temperature distribution for a 2D RM simulation on a grid of 480 x 120 points.

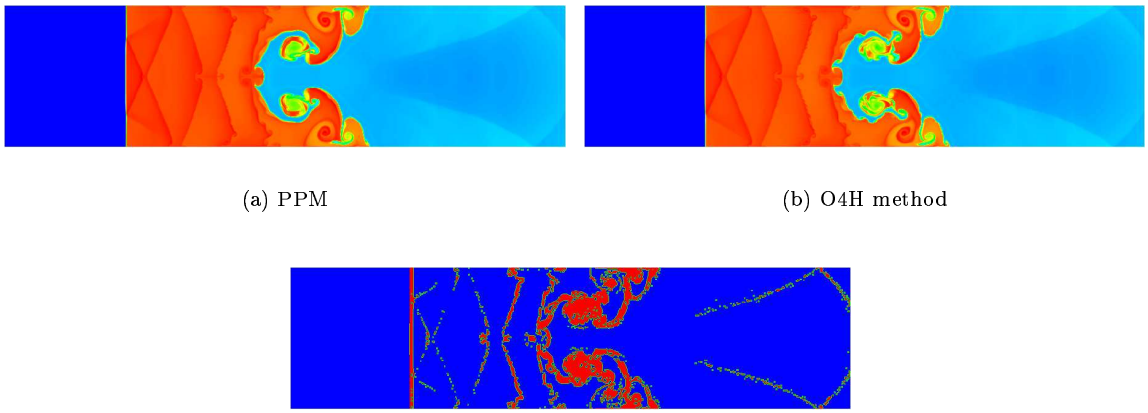

(a) PPM

(b) O4H method

(c) Switch locations

Figure 7. Temperature distribution for a 2D RM simulation on a grid of 960 x 240 points.

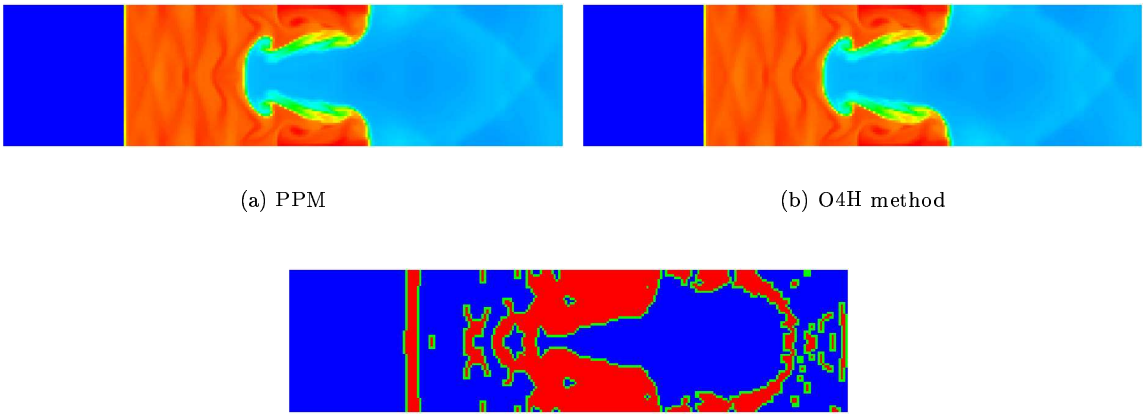

(a) PPM

(b) O4H method

(c) Switch locations

Figure 8. Temperature distribution in the central $x-y$ plane for a 3D RM simulation on a 240 x 60 x 60 grid. The PPM fluxes were used at the points shown as red in (c), the SM-FV fluxes were used in the blue regions, and the regions marked as green show where the average of the two fluxes were used.

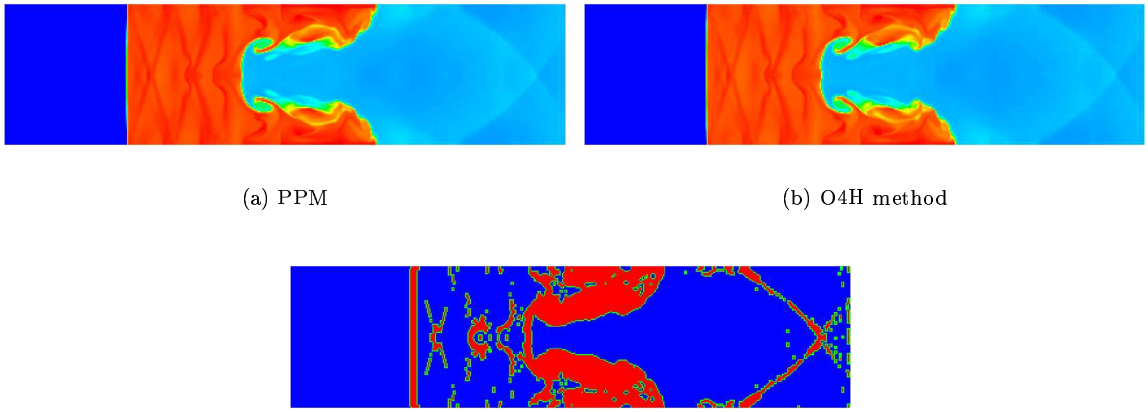

(a) PPM

(b) O4H method

(c) Switch locations

Figure 9. Temperature distribution along the central $x-y$ plane for a 3D RM simulation on a grid of 480 x 120 x 120.

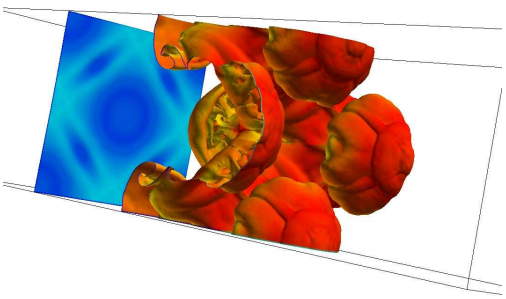

Figure 10. Temperature isosurface plot for the 3D RM simulation on a 480 x 120 x 120 grid. The shock is represented by the blue plane at the left.